

# New parameterization of the effective field theory motivated relativistic mean field model

Bharat Kumar<sup>a,b</sup>, S. K. Singh<sup>c</sup>, B. K. Agrawal<sup>b,d</sup>, S. K. Patra<sup>a,b\*</sup>

<sup>a</sup>*Institute of Physics, Sachivalaya Marg, Bhubaneswar - 751005, India.*

<sup>b</sup>*Homi Bhabha National Institute, Anushakti Nagar, Mumbai - 400094, India.*

<sup>c</sup>*Department of Physics, Indian Institute of Technology Roorkee, Roorkee 247667, India.*

<sup>d</sup>*Saha Institute of Nuclear Physics, 1/AF, Bidhannagar, Kolkata - 700064, India.*

---

## Abstract

A new parameter set is generated for finite and infinite nuclear system within the effective field theory motivated relativistic mean field (ERMF) formalism. The isovector part of the ERMF model employed in the present study includes the coupling of nucleons to the  $\delta$  and  $\rho$  mesons and the cross-coupling of  $\rho$  mesons to the  $\sigma$  and  $\omega$  mesons. The results for the finite and infinite nuclear systems obtained using our parameter set are in harmony with the available experimental data. We find the maximum mass of the neutron star to be  $2.03M_{\odot}$  and yet a relatively smaller radius at the canonical mass, 12.69 km, as required by the available data.

*Keywords:* Nuclear structure models, Binding energies and masses, Symmetry energy, Nuclear matter aspects of neutron star

*PACS:* 21.60.-n, 21.10.Dr, 21.65.Ef, 26.60.-c

---

## 1. Introduction

The nuclear physics inputs are essential in understanding the properties of dense objects like neutron stars. The relativistic mean field models based on the effective field theory (ERMF) motivated Lagrangian density have been instrumental in describing the neutron star properties, since, the ERMF models enables one to readily include the contributions from various degrees of freedoms such as hyperons, kaons and Bose condensates. The model parameters are obtained by adjusting them to reproduce the experimental data on the bulk properties for a selected set of finite nuclei. However, these parameterizations give remarkable results for bulk properties such as binding energy, quadrupole moment, root mean square radius not only for beta stable nuclei, but also for nuclei away from the stability line [1, 2]. However, the same model, sometimes does not appropriately reproduce the behavior of the symmetric nuclear matter and pure neutron matter at supra-normal densities as well as those for the pure neutron matter at the sub-saturation densities.

The ERMF model usually includes the contributions from the self and cross-couplings of isoscalar-scalar  $\sigma$ , isoscalar-vector  $\omega$  and isovector-vector  $\rho$  mesons. The inclusion of various self and cross-couplings makes the model flexible to accommodate various phenomena associated with the finite nuclei and neutron stars adequately without compromising the quality of the fit to those data considered a priori. For example, the self-coupling of  $\sigma$  mesons remarkably reduces the nuclear matter incompressibility to the desired values [3]. The cross-coupling

of  $\rho$  mesons with  $\sigma$  or  $\omega$  allows one to vary the neutron-skin thickness in a heavy nucleus like  $^{208}\text{Pb}$  over a wide range [4, 5]. These cross-couplings are also essential to produce desired behavior for the equation of state of pure neutron matter. Though, the effects are marginal, but, the quantitative agreement with the available empirical informations call for them [5, 6].

One may also consider the contributions due to the couplings of the meson field gradients to the nucleons as well as the tensor coupling of the mesons to the nucleons within the ERMF model [2]. These additional couplings are required from the naturalness view point, but very often they are neglected. Only the parameterizations of the ERMF model in which the contributions from gradient and tensor couplings of mesons to the nucleons considered are the  $\text{TM1}^*$ , G1 and G2 [2, 7]. However, these parameterizations display some disconcerting features. For instance, the nuclear matter incompressibility and/or the neutron-skin thickness associated with the  $\text{TM1}^*$ , G1 and G2 parameter sets are little too large in view of their current estimates based on the measured values for the isoscalar giant monopole and the isovector giant dipole resonances in the  $^{208}\text{Pb}$  nucleus [8, 9]. The equation of state (EoS) for the pure neutron matter at sub-saturation densities show noticeable deviations with those calculated using realistic approaches.

In the present paper, our motivation is to construct a new parameter set taking into account the multiple cross-couplings as well as the addition of  $\delta$ -meson which are generally ignored. Our new parameterization is confronted with the EoS for the symmetric and pure neutron matters available from diverse sources which indicate that the proposed parameter set can be employed to model the finite nuclei as well as the neutron stars.

The paper is organized as follows. Sec. 2 is devoted to a brief outline of the extended relativistic mean-field model. After get-

---

\*Corresponding author

Email address: patra@iopb.res.in (S. K. Patra<sup>a,b</sup>)

ting our newly generated parameter set, we have calculated the bulk properties of finite nuclei, nuclear matter and neutron star in Sec. 3. Finally, the concluding remarks are given in Sec. 4.

## 2. The model

Here, we start with the energy density functional for the ERMF model which includes the contributions from  $\delta$ -meson to the lowest order and the cross-coupling between  $\omega$  and  $\rho$  mesons which were not considered earlier by TM1\*, G1 and G2 parameterizations. The energy density functional can be written as [2, 7, 10],

$$\begin{aligned}
\mathcal{E}(r) = & \sum_{\alpha} \varphi_{\alpha}^{\dagger}(r) \left\{ -i\alpha \cdot \nabla + \beta [M - \Phi(r) - \tau_3 D(r)] \right. \\
& + W(r) + \frac{1}{2} \tau_3 R(r) + \frac{1 + \tau_3}{2} A(r) \\
& - \frac{i\beta\alpha}{2M} \cdot \left( f_{\omega} \nabla W(r) + \frac{1}{2} f_{\rho} \tau_3 \nabla R(r) + \lambda \nabla A \right) \\
& + \frac{1}{2M^2} (\beta_{\sigma} + \beta_{\omega} \tau_3) \Delta A \left. \right\} \varphi_{\alpha}(r) \\
& + \left( \frac{1}{2} + \frac{\kappa_3}{3!} \frac{\Phi(r)}{M} + \frac{\kappa_4}{4!} \frac{\Phi^2(r)}{M^2} \right) \frac{m_s^2}{g_s^2} \Phi^2(r) \\
& - \frac{\zeta_0}{4!} \frac{1}{g_{\omega}^2} W^4(r) + \frac{1}{2g_s^2} \left( 1 + \alpha_1 \frac{\Phi(r)}{M} \right) (\nabla \Phi(r))^2 \\
& - \frac{1}{2g_{\omega}^2} \left( 1 + \alpha_2 \frac{\Phi(r)}{M} \right) (\nabla W(r))^2 \\
& - \frac{1}{2} \left( 1 + \eta_1 \frac{\Phi(r)}{M} + \frac{\eta_2}{2} \frac{\Phi^2(r)}{M^2} \right) \frac{m_{\omega}^2}{g_{\omega}^2} W^2(r) \\
& - \frac{1}{2e^2} (\nabla A(r))^2 - \frac{1}{2g_{\rho}^2} (\nabla R(r))^2 \\
& - \frac{1}{2} \left( 1 + \eta_{\rho} \frac{\Phi(r)}{M} \right) \frac{m_{\rho}^2}{g_{\rho}^2} R^2(r) \\
& - \frac{\eta_{2\rho}}{4M^2} \frac{m_{\rho}^2}{g_{\rho}^2} (R^2(r) \times W^2(r)) \\
& + \frac{1}{2g_{\delta}^2} (\nabla D(r))^2 + \frac{1}{2} \frac{m_{\delta}^2}{g_{\delta}^2} (D^2(r)) \\
& - \frac{1}{2e^2} (\nabla A)^2 + \frac{1}{3g_{\gamma}g_{\omega}} A\Delta W + \frac{1}{g_{\gamma}g_{\rho}} A\Delta R. \quad (1)
\end{aligned}$$

The extended energy density functional with  $\delta$ -meson contains the nucleons and other exchange mesons like  $\sigma$ ,  $\omega$  and  $\rho$ -meson and photon  $A_{\mu}$ . The effects of the  $\delta$ -meson to the bulk properties of finite nuclei are nominal, but, the effects are significant for the highly asymmetric dense nuclear matter. The  $\delta$ -meson splits the effective masses of proton and neutron which influences the production of  $K^{+,-}$  and  $\pi^{+}/\pi^{-}$  in the heavy ion collision (HIC) [11]. Also, it increases the proton fraction in  $\beta$ -stable matter and modifies the transport properties of neutron star and heavy ion reaction [12, 13, 14]. Furthermore, in Eq.1, the terms having  $g_{\gamma}$ ,  $\lambda$ ,  $\beta_{\sigma}$  and  $\beta_{\omega}$  are responsible for the

effects related with the electromagnetic structure of the pion and nucleon [7]. We need to get the constant  $\lambda$  to reproduce the magnetic moments of the nuclei and is defined by

$$\lambda = \frac{1}{2} \lambda_p (1 + \tau_3) + \frac{1}{2} \lambda_n (1 - \tau_3) \quad (2)$$

with  $\lambda_p = 1.793$  and  $\lambda_n = -1.913$  the anomalous magnetic moments for the proton and neutron, respectively [7].

Certainly, the pairing correlation plays an important role for open-shell nuclei. The effect can not be ignored especially for heavy mass nuclei because the availability of quasi-particles states near the Fermi surface. The simple BCS approximation is an appropriate formalism for nuclei near the stability line. However, it breaks down for nuclei far away from it. The reason behind such anomaly is the number of protons/neutrons increases as it goes away from the stability valley. For such nuclei the Fermi level approaches zero and the number of available levels above the Fermi surface decreases. In this situation, the particle-hole and pair excitations reach the continuum. To overcome this problem, the BCS formalism is modified [15, 16] in an approximate manner by including the quasibound states (i.e., states bound by their centrifugal-plus-Coulomb barrier). In this present calculations, we have used the quasibound-BCS approach as done in Ref. [17] to take care of the pairing interaction.

## 3. Results and Discussions

We have calibrated the parameters of the energy density functional as given by Eq.(1). The optimization of the energy density functional is performed for a given set of fit data using the simulated annealing method. This method allows one to search for the best fit parameter in a given domain of the parameter space. The detailed procedure of the parameterization is given in Refs. [6, 18]. We have fitted the parameters or the coupling constants to the properties of few spherical nuclei together with some constraints on the properties of the nuclear matter at the saturation density. The experimental data for the binding energies and the charge radii for  $^{16}\text{O}$ ,  $^{40}\text{Ca}$ ,  $^{48}\text{Ca}$ ,  $^{68}\text{Ni}$ ,  $^{90}\text{Zr}$ ,  $^{100,132}\text{Sn}$  and  $^{208}\text{Pb}$  nuclei are used to fit the model parameters. The values of nuclear matter incompressibility  $K_{\infty}$  and symmetry energy coefficient  $J$  are constrained within 210–245 MeV and 28–35 MeV respectively. The parameter  $\zeta_0$  corresponding to the self-coupling of  $\omega$  mesons is allowed to vary within 1.0 – 1.5 in order to ensure that the maximum neutron star mass is  $\sim 2M_{\odot}$ . The obtained parameter set G3 along with other successful parameterizations NL3 [19], FSUGold2 [20], FSUGarnet [21] and G2 [7] are compared in Table 1. The NL3 is an old parameter set which has been popularly used. It includes self-coupling terms only for  $\sigma$  mesons and all the cross-coupling terms are ignored. The FSUGold2 and FSUGarnet on the other hand in addition includes cross-coupling between  $\omega$  and  $\rho$  mesons as well as the self-coupling term for the  $\omega$  meson. The G2 parameter set includes all the terms present in Eq. (1) except those corresponding to the  $\delta$ -meson and  $\omega$ - $\rho$  couplings.

Table 1: The obtained new parameter set G3 along with NL3 [19], FSUGold2 [20], FSUGarnet [21] and G2 [7] sets are listed. The nucleon mass  $M$  is 939.0 MeV. All the coupling constants are dimensionless, except  $k_3$  which is in  $\text{fm}^{-1}$ . The lower portion of the table indicates the nuclear matter properties such as binding energy per nucleon  $\mathcal{E}_0$ (MeV), saturation density  $\rho_0$ ( $\text{fm}^{-3}$ ), incompressibility coefficient for symmetric nuclear matter  $K_\infty$ (MeV), effective mass ratio  $M^*/M$ , symmetry energy  $J$ (MeV) and linear density dependence of the symmetry energy  $L$ (MeV).

	NL3	FSUGold2	FSUGarnet	G2	G3
$m_s/M$	0.541	0.530	0.529	0.554	0.559
$m_\omega/M$	0.833	0.833	0.833	0.832	0.832
$m_\rho/M$	0.812	0.812	0.812	0.820	0.820
$m_\delta/M$	0.0	0.0	0.0	0.0	1.043
$g_s/4\pi$	0.813	0.827	0.837	0.835	0.782
$g_\omega/4\pi$	1.024	1.079	1.091	1.016	0.923
$g_\rho/4\pi$	0.712	0.714	1.121	0.755	0.962
$g_\delta/4\pi$	0.0	0.0	0.0	0.0	0.160
$k_3$	1.465	1.231	1.368	3.247	2.606
$k_4$	-5.688	-0.205	-1.397	0.632	1.694
$\zeta_0$	0.0	4.705	4.410	2.642	1.010
$\eta_1$	0.0	0.0	0.0	0.650	0.424
$\eta_2$	0.0	0.0	0.0	0.110	0.114
$\eta_\rho$	0.0	0.0	0.0	0.390	0.645
$\eta_{2\rho}$	0.0	0.401	50.698	0.0	33.250
$\alpha_1$	0.0	0.0	0.0	1.723	2.000
$\alpha_2$	0.0	0.0	0.0	-1.580	-1.468
$f_\omega/4$	0.0	0.0	0.0	0.173	0.220
$f_\rho/4$	0.0	0.0	0.0	0.962	1.239
$\beta_\sigma$	0.0	0.0	0.0	-0.093	-0.087
$\beta_\omega$	0.0	0.0	0.0	-0.460	-0.484
<hr/>					
$\mathcal{E}_0$	-16.29	-16.28	-16.23	-16.07	-16.02
$\rho_0$	0.148	0.1505	0.1529	0.153	0.148
$K_\infty$	271.5	238.0	229.5	215.0	243.9
$M^*/M$	0.595	0.593	0.578	0.664	0.699
$J$	37.40	37.62	30.95	36.4	31.8
$L$	118.6	112.9	51.04	100.0	47.3

A detailed account on the importance of various couplings can be obtained in Refs. [2, 22, 23, 24].

The parameters, such as  $\eta_1, \eta_2, \eta_{2\rho}, \alpha_1, \alpha_2, f_\omega$  have their own importance to explain various properties of finite nuclei and nuclear matter. For instance, the surface properties of finite nuclei is analyzed through non-linear interactions of  $\eta_1$  and  $\eta_2$  as discussed in Ref. [2]. It is known that addition of the isovector  $\delta$ -meson softens the symmetry energy at subsaturation densities and it stiffens the EoS at high densities [25, 10]. The  $\delta$ -meson does not significantly modify the properties of finite nuclei, but it affects the maximum mass of the neutron-star and some other properties for highly asymmetric systems. Though, relevance of most of these parameters has been pointed out in Ref. [2] but, a more quantitative version along this direction, such as the uncertainties on the parameters and the correlations among the parameters, needs to be pursued within the covariance approach [20, 26]. An appropriate covariance analysis for the model considered in the present work requires a set of fitting data which includes large variety of nuclear and neutron star observables. The parameter obtained in the present work will facilitate such an investigation.

The computed results for NL3, FSUGold2, FSUGarnet, G2 and G3 are listed in Table 2. The binding energy per nucleon (B/A), root mean square charge radius  $R_c$  and neutron-

Table 2: The binding energy per nucleon B/A(MeV), charge radius  $R_c$  (fm) and neutron skin thickness  $R_n - R_p$  (fm) for some close shell nuclei compared with the NL3, FSUGold2, FSUGarnet, G2 and G3 with experimental data [27, 28].

Nucleus	Obs.	Expt.	NL3	FSUGold2	FSUGarnet	G2	G3
<sup>16</sup> O	B/A	7.976	7.917	7.862	7.876	7.952	8.037
	$R_c$	2.699	2.714	2.694	2.690	2.718	2.707
	$R_n - R_p$	-	-0.026	-0.026	-0.028	-0.028	-0.028
<sup>40</sup> Ca	B/A	8.551	8.540	8.527	8.528	8.529	8.561
	$R_c$	3.478	3.466	3.444	3.438	3.453	3.459
	$R_n - R_p$	-	-0.046	-0.047	-0.051	-0.049	-0.049
<sup>48</sup> Ca	B/A	8.666	8.636	8.616	8.609	8.668	8.671
	$R_c$	3.477	3.443	3.420	3.426	3.439	3.466
	$R_n - R_p$	-	0.229	0.235	0.169	0.213	0.174
<sup>68</sup> Ni	B/A	8.682	8.698	8.690	8.692	8.682	8.690
	$R_c$	-	3.870	3.846	3.861	3.861	3.892
	$R_n - R_p$	-	0.262	0.268	0.184	0.240	0.190
<sup>90</sup> Zr	B/A	8.709	8.695	8.685	8.693	8.684	8.699
	$R_c$	4.269	4.253	4.230	4.231	4.240	4.276
	$R_n - R_p$	-	0.115	0.118	0.065	0.102	0.068
<sup>100</sup> Sn	B/A	8.258	8.301	8.282	8.298	8.248	8.266
	$R_c$	-	4.469	4.453	4.426	4.470	4.497
	$R_n - R_p$	-	-0.073	-0.075	-0.078	-0.079	-0.079
<sup>132</sup> Sn	B/A	8.355	8.371	8.361	8.372	8.366	8.359
	$R_c$	4.709	4.697	4.679	4.687	4.690	4.732
	$R_n - R_p$	-	0.349	0.356	0.224	0.322	0.243
<sup>208</sup> Pb	B/A	7.867	7.885	7.881	7.902	7.853	7.863
	$R_c$	5.501	5.509	5.491	5.496	5.498	5.541
	$R_n - R_p$	-	0.283	0.288	0.162	0.256	0.180

skin thickness  $R_n - R_p$  for some selected nuclei are compared with experimental data, wherever available. From the table, it seems that the predictive power of the new set G3 for the nuclei considered in the fitting procedure is as good as for the NL3, FSUGold2, FSUGarnet and G2 sets. In Fig. 1 we plot the differences between the calculated and experimental binding energies for 70 spherical nuclei [29] obtained using different parameter sets. The triangles, stars, squares, diamonds and circles are the results for the NL3, FSUGold2, FSUGarnet, G2 and G3 parameterizations, respectively. The above results affirm that G3 set reproduces the experimental data better. The rms deviations for the binding energy as displayed in Fig. 1 are 2.977, 3.062, 3.696, 3.827 and 2.308 MeV for NL3, FSUGold2, FSUGarnet, G2 and G3 respectively. The rms error on the binding energy for G3 parameter set is smaller in comparison to other parameter sets.

In Fig. 2, the isotopic shift  $\Delta r_c^2$  for Pb nucleus is shown. The isotopic shift is defined as  $\Delta r_c^2 = R_c^2(A) - R_c^2(208)$  ( $\text{fm}^2$ ), where  $R_c^2(208)$  and  $R_c^2(A)$  are the mean square radius of <sup>208</sup>Pb and Pb isotopes having mass number A. From the figure, one can see that  $\Delta r_c^2$  increases with mass number monotonously till A=208 ( $\Delta r_c^2 = 0$  for <sup>208</sup>Pb) and then gives a sudden kink. It was first pointed by Sharma et al [30], that the non-relativistic parameterization fails to show this effect. However, this effect is well explained when a relativistic set like NL-SH [30] is used. The NL3, FSUGold2, FSUGarnet, G2 and G3 sets also appropriately predict this shift in Pb isotopes, but the agreement with experimental data of the present parameter set G3 is marginally better.

The differences in the rms radii of neutron and proton distribution,  $\Delta r_{np} = R_n - R_p$ , the so-called neutron-skin thickness are plotted in Fig. 3 for  $^{40}\text{Ca}$  to  $^{238}\text{U}$  for NL3, FSUGold2, FSUGarnet, G2 and G3 parameter sets as a function of proton-neutron asymmetry  $I = (N - Z)/A$ . The experimental data are also shown in the figure. Trzcińska et al. extracted the neutron-skin thickness of 26 stable nuclei ranging from  $^{40}\text{Ca}$  to  $^{238}\text{U}$  from experiments done with antiprotons at CERN [31, 32]. Keen observation on the data reveals more or less a linear dependence of neutron-skin thickness on the relative neutron excess  $I$  of nucleus. This can be fitted by [31, 32, 33]

$$\Delta r_{np} = (0.90 \pm 0.15)I + (-0.03 \pm 0.02)fm \quad (3)$$

Eq.3 is graphically represented in Fig. 3 by the orange shaded region. Most of the  $\Delta r_{np}$  obtained with NL3, FSUGold2, and G2 overestimate the data and deviate from the shaded region. On the other hand, the  $\Delta r_{np}$  calculated using G3 and FSUGarnet lie in side the shaded region. Interestingly, larger

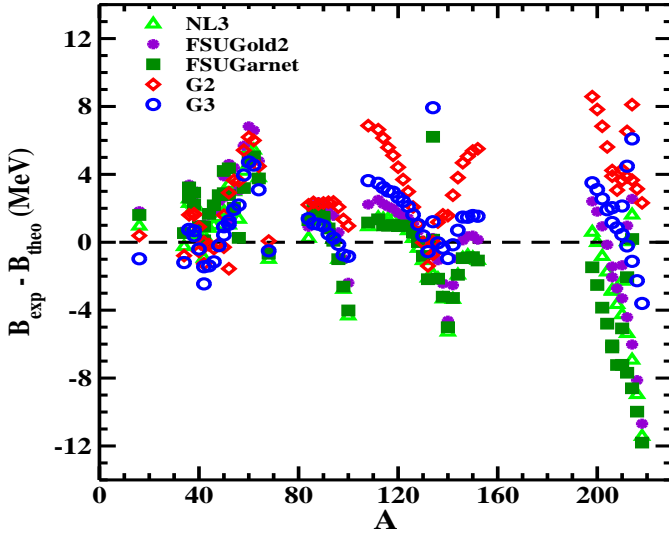


Figure 1: (color online) Difference between experimental and theoretical binding energies as a function of mass numbers for NL3 [19], FSUGold2 [20].

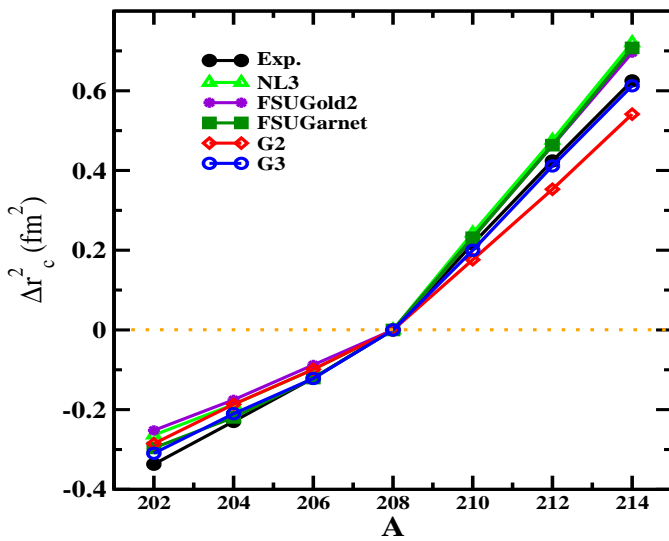


Figure 2: (color online) The isotopic shift  $\Delta r_c^2 = R_c^2(208) - R_c^2(A)$  (fm<sup>2</sup>) of Pb isotopes taking  $R_c$  of  $^{208}\text{Pb}$  as the standard value. Calculations with the NL3 [19], FSUGold2 [20], FSUGarnet [21], G2 [7] and G3 parameter sets are compared.

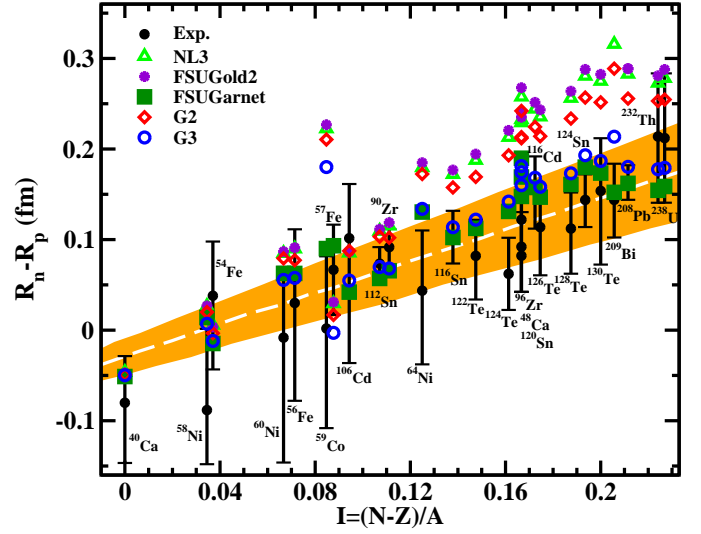


Figure 3: (color online) The difference in neutron and proton rms radii  $\Delta r_{np}$  obtained for NL3, FSUGold2, FSUGarnet, G2 and G3 are plotted as a function of isospin asymmetric  $I = (N - Z)/A$ . The experimental data displayed are taken from [31, 32]. The orange shaded region represents Eq. (3).

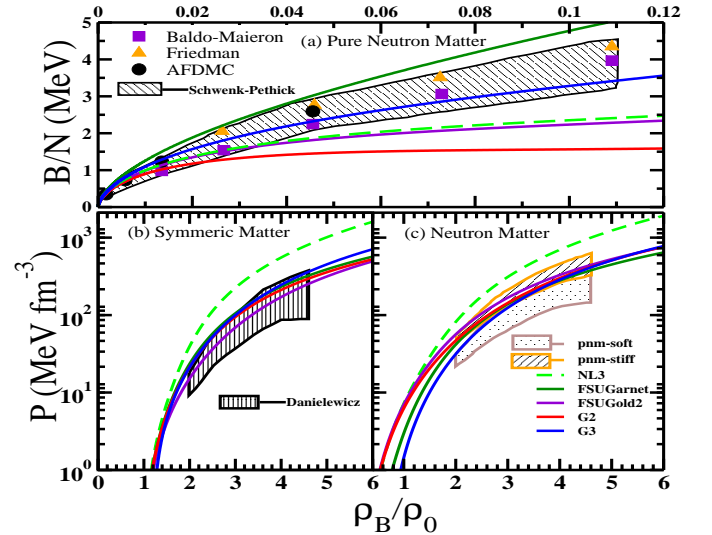


Figure 4: (color online) (a) The binding energy per neutron as a function of neutron density for G3 force is compared with other theoretical calculations along with experimental data [34, 35] for the region of sub-saturation density. (b) and (c) are the pressure versus baryon density for symmetric nuclear matter and pure neutron matter at high densities, respectively. The experimental data for higher density region are taken from [36].

experimental data. The overestimation of  $\Delta r_{np}$  for NL3, FSUGold2, and G2 parameter sets is due to the absence (or negligible strength) of  $\omega - \rho$  cross-coupling [4]. This term plays a crucial role in the determination of neutron distribution radius  $R_n$  without affecting much other properties of finite nuclei. It is shown in Ref. [37] that the derivative of neutron matter EoS at a sub-saturation density is strongly correlated with the  $\Delta r_{np}$ . Further, one can readily verify that the behavior of the neutron matter EoS should also depend on the incompressibility coefficient  $K_\infty$ , since, the energy per nucleon for an asymmetric matter can be decomposed into that for the symmetric nuclear matter and the density dependent symmetry energy within a quadratic approximation. Earlier parameterizations like TM1\*, G1 and G2 corresponding to the Lagrangian density similar to the one used in the present work yield higher values of  $K_\infty$  and/or  $J$ . In the present work, we have attempted to improve this short coming and constructed the force parameter G3 comprising  $J = 31.8$  MeV and  $K_\infty = 243.9$  MeV (see Table 2).

Our results for infinite symmetric nuclear and pure neutron matters are shown in Fig 4. The experimental data and predictions of other theoretical approaches are also plotted for comparison. Fig. 4(a), displays the energy per neutron in pure neutron matter at sub-saturation densities, which are encountered in finite nuclei and in clusterization of nucleons. The results for parameter sets NL3, FSUGold2, FSUGarnet and G2 deviate significantly from the shaded region. The non-relativistic forces labelled as Baldo-Maieron, Friedman, AFDMC are designed for sub-saturated matter density, however, they are not tested for the various mass regions of finite nuclei. The trend for the energy per neutron in pure neutron matter at low densities obtained by our parameter set G3 passes well through the shaded region. The EoS for symmetric matter and pure neutron matter are shown in Fig. 4(b) and Fig. 4(c), respectively for various parameter sets. Except the NL3, all other EOSs for the SNM and PNM obtained using FSUGold2, FSUGarnet, G2 and G3 are passing through the shaded region. Such a study by Arumugam et al [38] reported that EoS at high density overestimates the experimental data in the absence of  $\omega$ -meson self coupling and some cross-couplings.

Finally, we use our parameter set to estimate the mass and radius of the static neutron star composed of neutrons, protons, electrons and muons. The matter is assumed to be in  $\beta$ -equilibrium and is charge neutral. The contributions of the crust EoS to the mass and the radius of the neutron star for a given central density are estimated using Ref. [39]. It is shown in Ref. [39] that the mass and radius of the core for a given central density together with the chemical potential at the core-crust transition density are enough to estimate reasonably well the thickness and the mass of the crust. We have used the core-crust transition density to be  $0.074 \text{ fm}^{-3}$  and the chemical potential at the transition point to be 951.72 MeV, which altogether results in the total maximum mass,  $M_{\text{max}} = 2.03M_\odot$ , and the corresponding radius  $R_{\text{max}} = 11.03$  km. The radius for the neutron star at the canonical mass is  $R_{1.4} = 12.69$  km. The contribution due to crust to the total mass is  $\sim 0.015M_\odot$  and those for the crust thickness at the maximum and the canonical masses are 0.39 and 1.06 km, respectively. These values of the crust thick-

nesses are in harmony with the ones obtained in Ref. [40] using appropriate EoSs for the inner and outer crusts. Most of the relativistic mean-field models, in the absence of  $\delta$ -mesons, which satisfy the observational constraint of  $2M_\odot$  yield  $R_{1.4} > 13$  km [41]. The model DDH $\delta$  [42] which includes the  $\delta$ -meson contributions yield  $R_{1.4}$  similar to the ones as presently obtained. Our value of  $M_{\text{max}}$  is consistent with maximum mass so far observed for neutron stars like PSR J1614-2230 has  $M = 1.97 \pm 0.04M_\odot$  [43] and PSR J0348+0432 has  $M = 2.01 \pm 0.04M_\odot$  [44]. The value of  $R_{1.4} = 12.69$  km is also in good agreement with the empirical value  $R_{1.4} = 10.7 - 13.1$  km, which is consistent with the observational analysis and the host of experimental data for finite nuclei [45].

#### 4. Conclusions

In conclusion, we improve the existing parameterizations of the ERMF model which includes couplings of the meson field gradients to the nucleons and the tensor couplings of the mesons to the nucleons in addition to the several self and cross-coupling terms. The nuclear matter incompressibility coefficient and/or symmetry energy coefficient associated with earlier parameterizations of such ERMF model were little too large which has been taken care in our new parameter set G3. The rms error on the total binding energy calculated for our parameter set is noticeably smaller than the commonly used parameter sets NL3, FSUGold2, FSUGarnet, and G2. The neutron-skin thicknesses for our parameterization calculated for nuclei over a wide range of masses are in harmony with the available experimental data. The neutron matter EoS at sub-saturation densities for G3 parameter set show reasonable improvement over other parameter sets considered. Our value for the maximum mass for the neutron star is compatible with the measurements and the radius of the neutron star with the canonical mass agree quite well with the empirical values. The smallness of  $R_{1.4}$  for G3 parameter set in comparison to those for the earlier parametrization of the relativistic mean-field models, which are compatible with the observational constraint of  $2M_\odot$ , is a desirable feature.

In the upcoming, we will perform a detailed covariance analysis for the model used in the present work and assess the uncertainties associated with various parameters. An appropriate covariance analysis of our model requires a set of fitting data which includes large variety of nuclear and neutron star observables. The G3 parameter obtained in the present work will facilitate such an investigation.

#### Acknowledgement:

S. K. Singh is supported by the Council of Scientific and Industrial Research, Government of India, via Project No. 03(1338)/15/EMR-II.

## References

- [1] Y. K. Gambhir, P. Ring, and A. Thimet, *Ann. Phys. (N.Y.)* **198** (1990) 132.
- [2] M. Del Estal, M. Centelles, X. Viñas and S. K. Patra, *Phys. Rev. C* **63** (2001) 024314.
- [3] J. Boguta and A. R. Bodmer, *Nucl. Phys. A* **292** (1977) 413.
- [4] B. G. Todd-Rutel and J. Piekarewicz, *Phys. Rev. Lett.* **95** (2005) 122501; C. J. Horowitz and J. Piekarewicz, *Phys. Rev. Lett.* **86** (2001) 5647; *Phys. Rev. C* **64** (2001) 062802 (R).
- [5] J. Piekarewicz, B. K. Agrawal, G. Coló, W. Nazarewicz, N. Paar, P. -G. Reinhard, X. Roca-Maza, and D. Vretenar, *Phys. Rev. C* **85** (2012) 041302(R).
- [6] B. K. Agrawal, A. Sulaksono, P. -G. Reinhard, *Nucl. Phys. A* **882** (2012) 1.
- [7] R. J. Furnstahl, B. D. Serot and H. B. Tang, *Nucl. Phys. A* **598** (1996) 539; R. J. Furnstahl, B. D. Serot and H. B. Tang, *Nucl. Phys. A* **615** (1997) 441.
- [8] D. Patel, U. Garg, M. Fujiwara, H. Akimune, G. P. A. Berg, M. N. Harakeh, M. Itoh, T. Kawabata, K. Kawase, B. K. Nayak, T. Ohta, H. Ouchi, J. Piekarewicz, M. Uchida, H. P. Yoshida, M. Yosoi, *Phys. Lett. B* **718** (2012) 447.
- [9] X. Roca-Maza, X. Viñas, M. Centelles, B. K. Agrawal, G. Coló, N. Paar, J. Piekarewicz, and D. Vretenar, *Phys. Rev. C* **92** (2015) 064304.
- [10] S. K. Singh, S. K. Biswal, M. Bhuyan, S. K. Patra, *Phys. Rev. C* **89** (2014) 044001.
- [11] G. Ferini, M. Colonna, T. Gaitanos and M. Di Toro, *Nucl. Phys. A* **762** (2005) 147.
- [12] H. Chiu and E. E. Salpeter, *Phys. Rev. Lett.* **12** (1964) 413.
- [13] J. N. Bahcall and R. A. Wolf, *Phys. Rev. Lett.* **14** (1965) 343.
- [14] J. M. Lattimer, C. J. Pethic, M. Prakash and P. Haensel, *Phys. Rev. Lett.* **66** (1991) 2701.
- [15] E. Chabanat, P. Bonche, P. Haensel, J. Meyer and R. Schaeffer, *Nucl. Phys. A* **635** (1998) 231.
- [16] N. Sandulescu, Nguyen Van Giai and R. J. Liotta, *Phys. Rev. C* **61** (2000) 061301(R).
- [17] M. Del Estal, M. Centelles, X. Viñas and S. K. Patra, *Phys. Rev. C* **63** (2001) 044321.
- [18] B. K. Agrawal, S. Shlomo, and V. Kim Au, *Phys. Rev. C* **72** (2005) 014310.
- [19] G. A. Lalazissis, J. König and P. Ring, *Phys. Rev. C* **55** (1997) 540.
- [20] Wei-Chai Chen and J. Piekarewicz, *Phys. Rev. C* **90**, (2014) 044305.
- [21] Wei-Chai Chen and J. Piekarewicz, *Phys. Lett. B* **748**, (2015) 284.
- [22] X. Roca-Maza, X. Viñas, M. Centelles, P. Ring, and P. Schuck, *Phys. Rev. C* **84** (2011) 054309.
- [23] N. Alam, A. Sulaksono, and B. K. Agrawal, *Phys. Rev. C* **92** (2015) 015804.
- [24] S. K. Biswal, S. K. Singh, M. Bhuyan and S. K. Patra, *Brazilian Journal of Physics*, **45** (2015) 347.
- [25] S. Kubis and M. Kutschera, *Phys. Lett. B* **399** (1997) 191.
- [26] Nikšić, N. Paar, P-G Reinhard and D. Vretnar, *J. Phys. G* **42** (2015) 034008.
- [27] M. Wang, G. Audi, A. H. Wapstra, F. G. Kondev, M. MacCormick, X. Xu and B. Pfeiffer, *Chin. Phys. C* **36** (2012) 1603.
- [28] I. Angeli, K. P. Marinova, *At. Data and Nucl. Data Tables* **99** (2013) 69.
- [29] P. Klüpfel, P. -G. Reinhard, T. J. Bürvenich, and J. A. Maruhn, *Phys. Rev. C* **79** (2009) 034310.
- [30] M. M. Sharma, G. A. Lalazissis and P. Ring, *Phys. Lett. B* **317** (1993) 9.
- [31] A. Trzcińska, J. Jastrzębski, P. Lubiński, F. J. Hartmann, R. Schmidt, T. von Egidy, and B. Klos, *Phys. Rev. Lett.* **87** (2001) 082501.
- [32] J. Jastrzębski, A. Trzcińska, P. Lubiński, B. Klos, F. J. Hartmann, T. von Egidy, S. Wycech, *Int. J. Mod. Phys. E* **13** (2004) 343.
- [33] X. Viñas, M. Centelles, X. Roca-Maza and M. Warda, *Eur. Phys. J. A* **50** (2014) 27.
- [34] Alexandros Gezerlis and J. Carlson, *Phys. Rev. C* **81** (2010) 025803.
- [35] M. Dutra, O. Lourenço, J. S. Sá Martins, A. Delfino, J. R. Stone and P. D. Stevenson, *Phys. Rev. C* **85** (2012) 035201.
- [36] P. Danielewicz et al., *Science* **298** (2002) 1592.
- [37] B. A. Brown, *Phys. Rev. Lett.* **85** (2000) 5296.
- [38] P. Arumugam, B. K. Sharma, P. K. Sahu, S. K. Patra, Tapas Sil, M. Centelles and X. Viñas, *Phys. Lett. B* **601** (2004) 51.
- [39] J. L. Zdunik, M. Fortin and P. Haensel, *Astron. Astrophys.* **599** (2017) 119.
- [40] Fabrizio Grill, Helena Pais, Constança Providência, Isaac Vidaña and Sidney S. Avancini, *Phys. Rev. C* **90** (2014) 045803.
- [41] N. Alam, B. K. Agrawal, M. Fortin, H. Pais, C. Providência, Ad. R. Raduta and A. Sulaksono, *Phys. Rev. C* **94** (2016) 052801(R).
- [42] T. Gaitanos, M. Di Toro, S. Typel, V. Baran, C. Fuchs, V. Greco and H.H. Wolter, *Nucl. Phys. A* **732** (2004) 24.
- [43] P. B. Demorest, T. Pennucci, S. M. Ransom, M. S. E. Roberts, and J. W. T. Hessels, *Nature (London)* **467** (2010) 1081.
- [44] J. Antoniadis et al., *Science* **340** (2013) 6131.
- [45] Lattimer and Y. Lim *Astrophys. J.* **771** (2013) 51.